Original Research Paper

Numerical and experimental investigations on new jar designs for high efficiency planetary ball milling

M. Broseghini [a,1], M. D'Incau [a], L. Gelisio [a,2], N.M. Pugno [b,c], P. Scardi [a,*]

[a] Department of Civil, Environmental & Mechanical Engineering, University of Trento, via Mesiano, 77, 38123 Trento, Italy
[b] Laboratory of Bio-inspired, Bionic, Nano, Meta Materials & Mechanics, Department of Civil, Environmental & Mechanical Engineering, University of Trento, via Mesiano, 77, 38123 Trento, Italy
[c] School of Engineering and Materials Science, Queen Mary University of London, Mile End Road, London E1 4NS, United Kingdom

ABSTRACT

The internal shape of planetary ball mill jars was modified to increase the efficiency of the milling process. Four new jar designs are presented, where obstacles on the surface of a traditional cylindrical jar modify the ratio of normal-to-tangential transferred mechanical action, thus improving the comminution of the mill charge and reducing the process time. Multibody dynamics simulations, validated by *operando* video recordings of the process, were employed to investigate modified ball motion regimes promoting the increase of the number of high-energy impacts. Moreover, experimental grinding of calcium fluoride powder was performed to assess the effect of milling time and jar-to-plate velocity ratio, through the evaluation of size and microstrain of the end product deduced from X-ray diffraction line profile analysis.
© 2020 The Society of Powder Technology Japan. Published by Elsevier B.V. and The Society of Powder Technology Japan. All rights reserved.

1. Introduction

Planetary ball mill is a widely used apparatus to process almost any class of material, from metals and ceramics to organic compounds and pharmaceuticals [1–6].

The geometry of the device and its working principle are rather simple, with grinding occurring by impacts between milling media (balls and jar) and mill charge (see *e.g.* [1,7]). Collisions intensity, direction, frequency and, consequently, the characteristics of the end product are determined by ball movements inside the jar, which in turn depend on the setup of many milling parameters. Optimization of these variables can be addressed experimentally [8–10] and/or through analytical [8,11] and numerical [9,12] modelling. While literature proposes several works analysing parameters such as the number and dimension of balls [13–15], the angular velocity of revolving parts [13,9,16,12], the balls filling ratio [16] and friction [9], much less attention is deserved to the shape of the jar, assumed generally to be cylindrical. This work investigates instead the effect of re-designing the internal shape

of the jar, deemed as an alternative and advantageous way to perturb the milling media trajectories and enhance the process efficiency.

Preliminary insights on the effectiveness of this variable are reported in [17,18], where a jar with half-moon cross section (HM) is proposed and compared with the standard cylindrical one (CY). The present work extends the analysis to other 3 shapes that break the cylindrical symmetry in different ways but pursue the same goal of increasing the number of high-energy impacts. Investigations are carried out through different approaches. In particular, multibody dynamics simulations of the process are exploited to compute the ball trajectories and velocities and to provide estimates of average kinetic impact energy. Validation of modelling predictions is then accomplished both directly by *operando* video recordings of the grinding process and indirectly by X-ray Powder Diffraction (XRPD) Line Profile Analysis (LPA) of ground calcium fluoride (CaF_2), employed to characterise the structure and microstructure of the end product.

2. Planetary ball mill and new jar designs

In a planetary ball mill two or more rotating (with angular velocity ω) jars, containing the grinding balls and the mill charge, are installed on a rotating (with angular velocity Ω) disk. The arising centrifugal and Coriolis forces drive ball motion, causing

---

a. Cylindrical (CY)   b. Half Moon (HM)   c. 1 Lifter (1L)   d. 3 Lifter (3L)   e. Triangular (T)
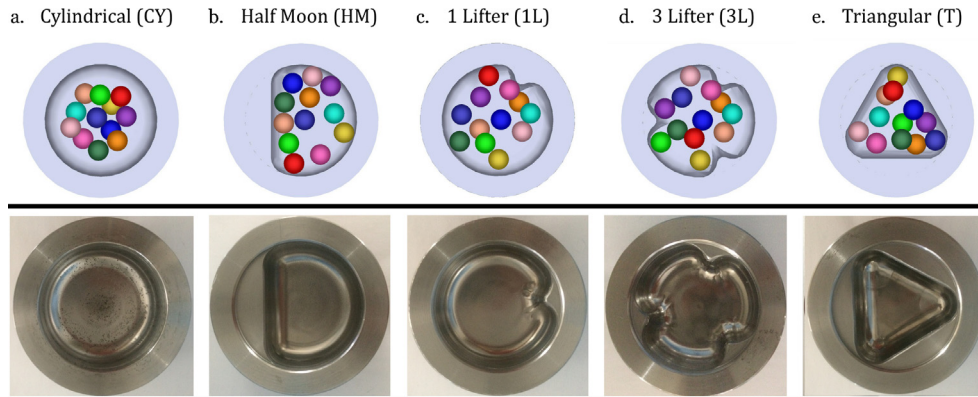
Fig. 1. Designs of the internal shape of the jar. Top, parasolid models for multibody dynamic simulations. Bottom, stainless steel jars.

impacts that transfer compressive and shear forces to the mill charge. Generally speaking, while shear actions produce plastic deformation, size reduction of powder particles (comminution) is promoted by compressive forces [19–21], exchanged in the axial direction with respect to the local impact reference frame, consisting of two axes, one normal and one tangential to the contact surface.

Trajectories of balls strictly relate to the setup of mill operational parameters, which determine whether they roll and slide or swirly cross the grinding chamber. Different motion regimes can therefore be recognized and, the more disordered they are, the higher the number and the intensity of the impacts [22,16]. An alternative approach to modify – and possibly improve – the milling process is to re-design the internal shape of the jar. Fig. 1 proposes 4 shapes that, in different ways, could enhance the amount of impacts with high normal-relative-velocity component and therefore improve the comminution of the mill charge. Particularly, the 1Lifter (1L) and the 3Lifters (3L) designs (Fig. 1c and 1d) were inspired by the tumbling ball mills (presenting a cylindrical lined shell) and introduce respectively 1 and 3 obstacles (lifters) along the jar wall. These shoot balls in different directions-depending on impact angles and velocities, therefore strongly disordering ball movements. The number of the lifters has to be properly planned: in fact, a high number of lifters enhances the ball motion disorder and the amount of collisions but, at the same time, it reduces the internal volume of the jar and, in turn, the maximum flight length and the velocity of balls. Lifters shape and dimension also deserves specific attention and, in particular, rounded profiles have to be preferred over sharp edges to prevent the formation of regions barely accessible by milling media where the powder could accumulate and therefore would not be milled.

The Half-Moon (HM) shape (Fig. 1b) was inspired by the theoretical analysis of the ideal trajectory of a single ball in a standard cylindrical jar (CY, Fig. 1a), proposed in literature [11]. Theory indeed suggests that a ball should move as an integral whole with a point on the vial circumference until, by a given composition of the inertial forces, it is launched against the opposite point, perpendicularly to the jar surface. This results in a high velocity impact, transferring a large amount of energy especially along the axial direction. However, in a real scenario, due to the interactions with many balls and the mill charge, this ideal trajectory hardly takes place. Therefore, the HM shape introducing a flat surface halfway between the curved wall and the axis of a CY jar was designed so to drive the balls along the above-described *ideal path*. Finally, the Triangular (T) jar (Fig. 1e) can be considered an amplification of the HM concept, as it presents 3 flat surfaces.

3. Methods

Newly designed jars were investigated through experiments performed in a planetary ball mill Fritsch Pulverisette 4 (P4, [23]) and by numerical simulations. Jar (ω) to plate (Ω) velocity ratio, expressed as $\omega/\Omega + 1$, was varied between 0.0 and −4.0 (with fixed Ω and ω counterrotating and increasing in magnitude) for each set of analysis.

12 carbon steel balls were placed inside stainless steel jars (geometrical and physical properties of the milling media as well as the internal volume of the jars are reported in Table 1).

For every jar, experiments were performed on calcium fluoride (CaF_2), grinding 2.1 g of powder under different velocity ratios for 32 h. Moreover, for the CY and HM jars, additional samples were ground for different milling time (1 h, 4 h, 8 h, 16 h, 32 h and 64 h) so to assess also the effect of this variable.

3.1. Camera recordings

Ball motion inside the jars was monitored *operando* by means of a high speed camera (Sony Action Cam HDR-AS200V, 240 fps, 1280X720 pixel resolution). As shown in Fig. 2, the camera was directly installed on the jar through an expressly designed slot.

Table 1
Geometrical and physical properties of jar and milling media and internal volume of the jars.

Jars (AISI 304)	
Internal radius	32.5 mm
External volume	80 cm³
Density	8.03 g/cm³
Young modulus	193 GPa
Poisson ratio	0.29
Spheres (AISI 1020)	
Number	12
Radius	6 mm
Density	7.85 g/cm³
Young modulus	200 GPa
Poisson ratio	0.29
Jars Internal Volume	
Cylindrical (CY)	72 cm³
Half Moon (HM)	60 cm³
1 Lifter (1L)	71 cm³
3 Lifters (3L)	69 cm³
Triangular (T)	51 cm³

Fig. 2. Left, slot used for mounting the high speed camera directly on the jar equipped with a transparent lid. Right, the complete system mounted in the P4 planetary ball mill.

Therefore, the recorded ball- trajectories refer to the vial reference frame. The visibility of milling media was allowed by a transparent (policarbonate) lid and 50 LEDs mounted on a ring (*i.e.* an automotive angel eye). A first group of recordings was taken without the mill feed. Later, calcium fluoride was added and a new batch of observations of the milling tests performed. In this way the effect of the mill charge was clearly highlighted. Both qualitative and quantitative information could in principle be extracted from camera recordings [10] but in this work, only a qualitative analysis of ball movements and their dependence on the jar shape and the velocity ratio is considered.

3.2. Computer simulations

New designed jars were tested through a multibody dynamics numerical model, developed within the framework of MSC.Adams software [24,25]. Impacts among the milling media (treated as rigid bodies) are the crucial ingredient of this model and were simulated by adding to the Lagrangian equations of motion a force–displacement law, expressed as a combination of a non-linear spring in parallel with a linear damper (hard-coded *impact* function [24]) [26,27].

Both for the ball-ball and the ball-jar impacts, the generalised stiffness k and the exponent n, describing the elastic part of this law, were deduced from the Hertz theory of contact [28]. For the dissipative part, an upper bound value for the damping coefficient c_{max} expressed as a function of compenetration of colliding bodies, was provided by the classical solution of the damped vibration of a mass-spring system [27]. The comparison between simulated and experimental results of a sphere-on-plate drop test allowed to tune the compenetration d at which c_{max} applies and to validate the reliability of the modelled description of the impact event (more details in [25,29]).

Friction at contact location was taken into account through the hard-coded regularised formulation of the Coulomb model [24], adopting a friction coefficient expressed as a function of the relative velocity of colliding bodies in tangential direction, smoothly varying from the static μ_s to the dynamic μ_d value, deduced respectively from literature and pin-on-disc tribological tests. As suggested in [9], the mill charge (CaF_2) was not explicitly modeled but indirectly accounted for by a suitable selection of these parameters, estimated for two boundary cases *i.e.* the (i) steel-steel (no mill charge) and the (ii) steel-fluorite interaction (*i.e.* jar or balls surface completely covered by the mill charge), as real grinding is expected to fall in-between these two extreme conditions. This allowed a direct comparison between simulations and camera movies of the steel-steel interaction and further speculations on the effect of the powder. Adopted contact and friction parameters are reported in [25].

The Hilbert-Hughes-Taylor (HHT, [30,31]) integrator with automatic timestep tuning and maximum numerical error of 10^{-8} was used to compute the solution of the equations of motion of the milling media. Simulations lasted 24s but the first 4s were discarded during data analysis so to disregard the motion homogenization phase.

In addition to the quantities characterising the motion of each body, also deducible from camera recordings, simulations output provided the complete description of contact events, largely inaccessible to experiments and of utmost importance for properly tuning the properties of the end product. In particular, in this work, the relative velocity of colliding bodies, divided into normal (axial) and tangential components with respect to the local impact reference frame, was exploited for the estimate of the average kinetic energy available.

3.3. X-ray powder diffraction

The effect of grinding on the calcium fluoride powder was assessed by X-ray Powder Diffraction Line Profile Analysis (XRPD-LPA, [32,33]). Data were collected on a Rigaku PMG/VH diffractometer, using CuKα radiation monochromatized by a pyrolytic graphite curved crystal in the diffracted beam (details on the measurement parameters can be found in [34]). LPA was based on the Whole Powder Pattern Modelling (WPPM) approach [35–37]. The analysis provided an average size $\langle D \rangle$ for the crystalline domains, assumed to be spherical and dispersed according to a log-normal distribution, and an average dislocation density ρ considering the primary slip system and the elastic constants of fluorite [38–43,2]. The analysis was based on the presence of one or two fractions of fluorite, depending on the efficiency of the specific grinding vial and milling conditions. Particularly, a single fluorite phase was considered when the milling product was a homogeneously fine powder, whereas an additional phase was introduced to model a coarse (little or not ground) powder fraction, present in varied percentages together with the fine fraction when the grinding process was not efficient or sufficiently long. Differently from our previous work on this subject, the WPPM model was included in software macros running in the Rietveld refinement software TOPAS (version 6, [44]), so to support the LPA by the structural model of the present phases, which acts as a constraint adding robustness and reliability to the analysis. In particular, besides the one or two fractions of fluorite (respectively fine and coarse), the analysis also considered a minor fraction of MgO (contaminant phase in the starting powder, around 0.5%), and the amount of steel contamination from the milling media, modelled as ferritic iron.

4. Results

In the first part of this section, the effect of re-designing the jar shape is investigated in terms of ball motion, energy exchange and grinding performance, together with its dependence on the jar-to-plate velocity ratio ($\omega/\Omega + 1$), through multibody dynamics simu-

lations and XRPD-LPA performed on samples of ground calcium fluoride. XRPD data are further exploited in the second part of the section to analyse the effect of milling time and its connection with the wear of milling media.

4.1. Effect of jar shape on ball motion, impact energy and comminution

Several works in literature [8,9,12,10] pointed out that in a planetary ball mill equipped with a standard cylindrical jar, 3 different ball motion regimes (cascading, cataracting, rolling) arise, depending on the jar-to-plate velocity ratio ($\omega/\Omega + 1$). Particularly, in [25] multibody dynamics simulations of the milling process (performed without mill feed, steel-steel interaction only) showed that, for the selected mill configuration, at lower (in magnitude) $\omega/\Omega + 1$ balls move along jar wall as a compact group into cascading motion. Later, at increasing jar velocity, they detach from the group and collide against other balls or the jar wall, gradually enhancing the motion disorder up to $\omega/\Omega + 1 = -2.6$, where it reaches the maximum complexity (*i.e.* randomness, cataracting regime). Above this threshold, a sharp change occurs and balls stick to jar surface (rolling mode). Owing to the larger number of high-velocity impacts, the cataracting mode was demonstrated to be the most effective in transferring energy to the mill charge [25] and, therefore, jars here presented (HM, 1L, 3L, T in Fig. 1 b, c, d, e) were designed so to promote this kind of motion. Simulations of the process and *operando* monitoring via camera recordings revealed that the motion of the milling media circulating in the new profiles is disordered already starting from lower values of $\omega/\Omega + 1$. More precisely, the beginning of the cataracting regime can be observed at approximately $\omega/\Omega + 1 = -1.8$ and it extends till -2.2, namely over a wider range than in the CY. This suggests that the jar shape has the strongest influence among the milling variables.

While the most significative movies can be found in Supplementary Material, selected pictures giving insights on motion modes detected for the CY and the 3L jars are reported in Fig. 3. Camera recordings are in good agreement with simulations, both in terms of motion regimes and their variation with $\omega/\Omega + 1$, thus validating the modelling results.

Simulations provided also the relative velocity of colliding bodies. A simple parameter proposed by several authors [9,45,1] that can be used to qualitatively compare the efficiency of the different jar shapes is the so-called Stress Energy (*SE*). This quantity can be calculated for each *k*-th collision and represents the maximum kinetic energy that can be involved in it [9,45,1]

$$SE_k = \frac{1}{2} \frac{m_i m_j}{m_i + m_j} \dot{u}^2, \qquad (1)$$

being m_i and m_j the masses of the *i*-th and *j*-th impacting bodies respectively (in ball-jar contacts $m_{jar} = \infty$ as $m_{jar} \gg m_{ball}$) and $\dot{u}$ their relative velocity at the beginning of the contact event, which can also be decomposed into normal ($\dot{u}_n$) and tangential ($\dot{u}_t$) components with respect to the local impact reference frame.

Due to the complexity of phenomena taking place during the ball milling process that can not be accounted for by the proposed model – e.g. changes in powder structure and morphology, heat transfer etc. –, the amount of energy effectively transferred to the mill feed is hardly estimable. Consequently, as proposed in literature [9,45,1], as a first order approximation the Stress Energy (Eq. (1)) is computed according to the stereomechanical law of energy loss for the perfectly plastic collision and thus corresponds to the maximum amount of energy that can be supplied to the mill charge particles by each contact. This quantity represents therefore the upper bound of the energy involved in an impact and it is not directly comparable with energy transferred to the mill charge in a real apparatus.
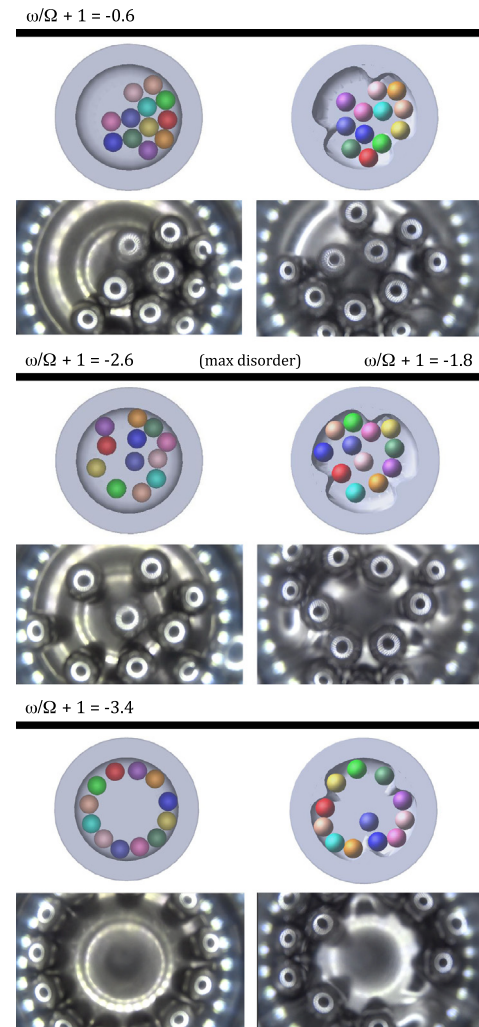
Fig. 3. Comparison of ball movements in the CY and 3L jars from simulations and camera recordings for 3 different $\omega/\Omega + 1$ ($\Omega = 50$ rpm), pointing out the existence of three different motion regimes. A good agreement between simulated and recorded images can be appreciated.

Furthermore it should be noticed that, within the proposed simulation framework, a continuous contact scheme is adopted to describe the collisions – i.e. the duration of the impact is assumed to be finite and not instantaneous – and therefore each contact is sampled by a certain amount of calculation points. The amount of points is however not known *a priori* but, at the aim of having the most accurate description of the contact, it varies for each collision depending on its complexity – i.e. impact angle and velocity, number of bodies involved etc. – and integrator settings. Thus, to compute Eq. (1), output data were filtered in order to account for the initial relative velocity only. The filter was designed according to the average duration of a two-body impact. Simulations of two spheres impacting at different angles and velocities were performed to estimate the reasonable maximum duration of a collision. Data time-wise shorter than this period were discarded from calculation (more details in [29]).

For each tested $\omega/\Omega + 1$ condition, the probability-weighted average of the Stress Energy (Eq. (1)) was computed, both in normal and tangential direction, and normalised over the internal volume *V* of the jars (see Table 1), to account for the different geometrical constraints in ball movements and velocity. This quantity estimates the average kinetic energy density involved in an impact and is reported in Fig. 4 both for the steel-steel (upper part)
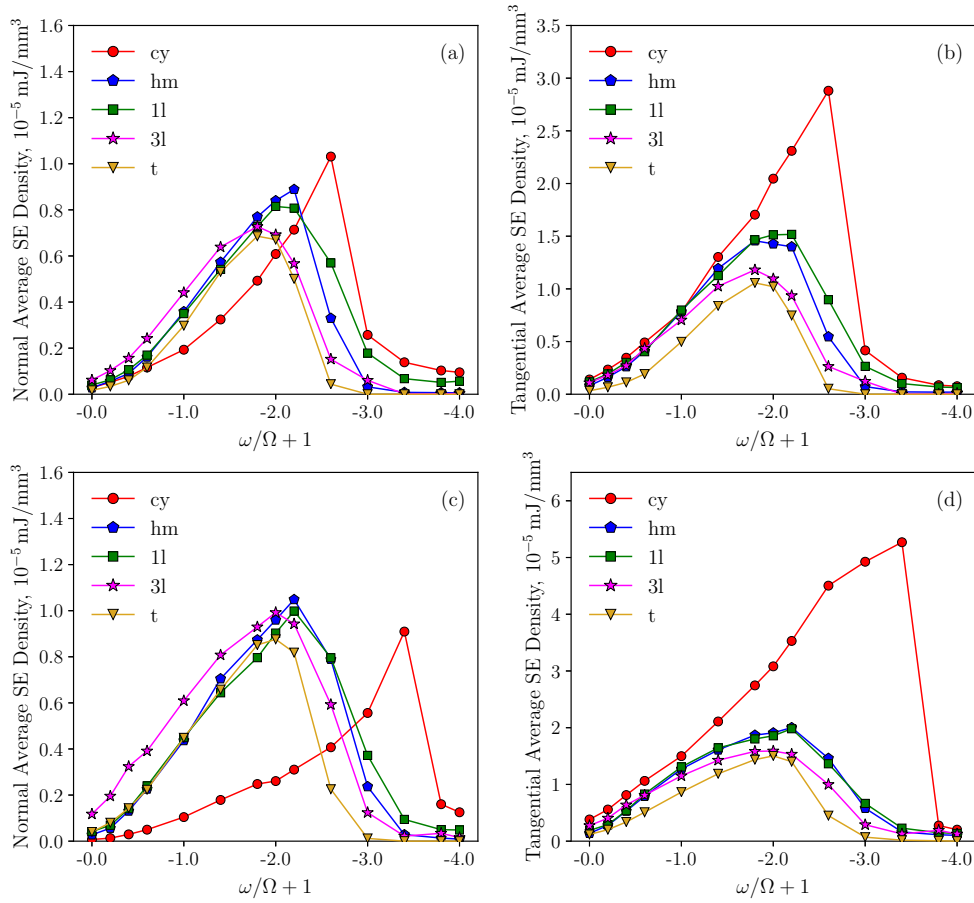
Fig. 4. Average stress energy density of impacts in normal (a, c) and tangential direction (b, d) for tested $\omega/\Omega + 1$. These quantities are shown for the steel-steel (a, b) and for the steel-fluorite interaction (c, d).

and the steel-fluorite (lower part) interactions, since real grinding conditions are expected to fall in between these two boundary cases (modelled by suitably modifying the friction parameters μ_s and μ_d, see Methods).

For the steel-steel case, both the normal and the tangential average impact energy components present a maximum peaked at $\omega/\Omega + 1 = -2.6$ for the CY and a range of almost comparable values extended from $\omega/\Omega + 1 = -1.8$ to -2.2 for the other jars (Fig. 4, a and b). These ranges of velocity ratios, optimal in terms of impact kinetic energy density, nicely agree with the conditions of most disordered ball motion revealed by camera recordings, thus evidencing the close relation between ball motion and available energy. Moreover, the reduced friction due to the presence of fluo-

rite, promotes an increase of the average energy density, especially in tangential direction, and a shift to more negative $\omega/\Omega + 1$ ratios of maximum stress energy. These effects are much less evident for the new design jars, thus confirming that the process is more affected by the jar shape than by the other milling variables, including the characteristics of the mill charge.

What is even more important to note is that the average energy density in normal direction (Fig. 4, a and c) is larger for the new design jars than for the CY, from the very low $\omega/\Omega + 1$ and up to approximately $\omega/\Omega + 1 = -2.6$, when the rolling begins. This relates to the greater disorder of ball movements that, as shown in the left part of Fig. 5, particularly enhances the number of
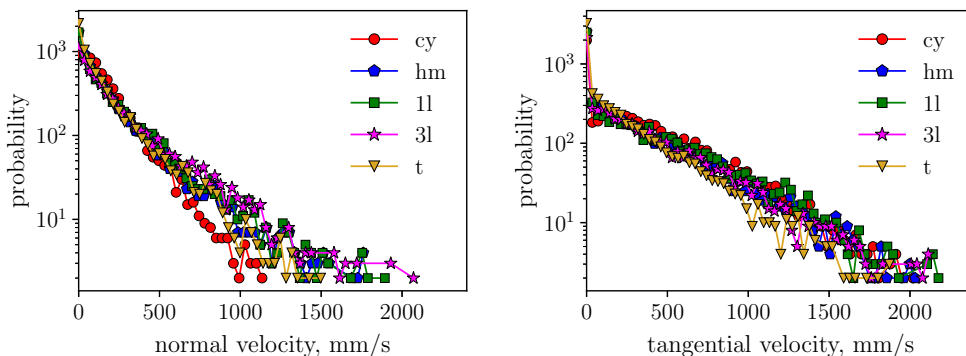
Fig. 5. Probability distributions of normal (left) and tangential (right) components of relative velocity of colliding bodies for $\omega/\Omega + 1 = -1$ ($\Omega = 200$ rpm). In normal direction, the new jars exhibit a larger number of high-velocity impacts than the CY. In tangential direction, instead, all the jars give comparable results.
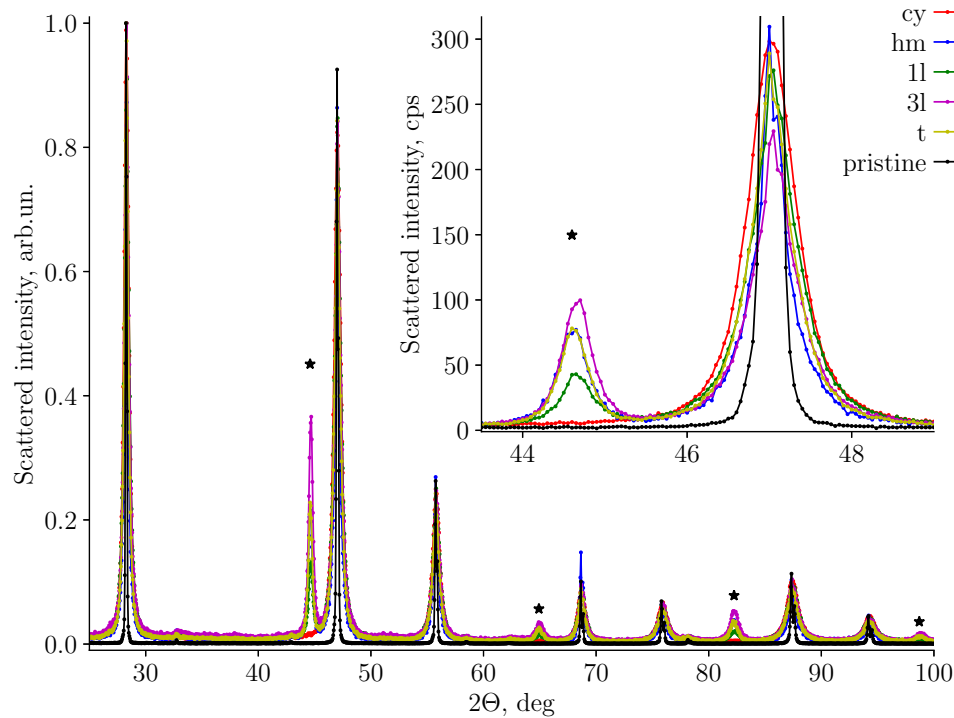
Fig. 6. A selection of representative XRPD patterns of CaF$_2$, pristine (black) and ground for 32 h with Ω = 200 rpm and $\omega/\Omega + 1$ = −2.6. All the patterns are normalized to the value of the [111] peak. The inset shows a magnification of the [220] peak (not normalized intensities). Stars indicate peaks resulting from the metal contamination from the milling media.
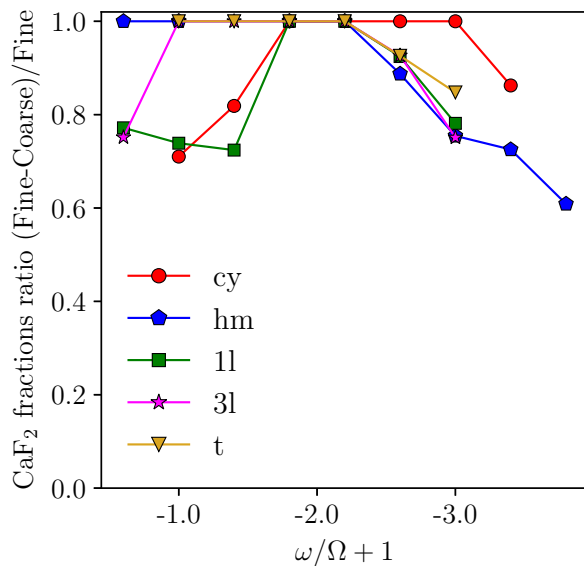
Fig. 7. Ratio of fine and coarse fractions of calcium fluoride ground for 32 h, under different velocity ratios and Ω=200 rpm. The presence of the coarse fraction implies incomplete/not efficient grinding, while a uniform end product indicates that proper milling conditions were adopted. Best milling conditions range from $\omega/\Omega + 1$ = −1.8 to −3.0 for the CY vial and from about −0.6 to −2.2 for the other jars.

200 rpm and $\omega/\Omega + 1$ = −2.6 in different jars is shown in 6 together with the pattern from the pristine powder. As anticipated in Section 3.3, in case of barely efficient grinding conditions the resulting powder is not homogeneous, showing the coexistence of a ground (fine) and a less-to-not ground (coarse) fractions, the ratio of which was provided by the LPA and is reported in Fig. 7. Interestingly and almost in line with simulations results, best grinding performances – *i.e.* conditions providing with a homogeneous and finely ground end product which can be modelled by a single distribution – range from approximately $\omega/\Omega + 1$ = −1.8 to −3.0 for the CY, whereas correspond to lower velocity ratios (from about −0.6 to −2.2) for the other jars. The 1L jar seems to behave differently from the other new design jars since a larger fraction of coarser powder can be detected for the lower velocity ratios (from $\omega/\Omega + 1$ = −0.6 to −1.4). However, LPA revealed that this fraction can not be actually considered as coarse, exhibiting smaller $\langle D \rangle$ (nanometer range) with respect to the coarse fraction produced by the CY. It can therefore be deduced that, although a slightly reduced homogeneity of the end product with respect to the other new design jars is shown, at low velocity ratios also the 1L performs well and, above all, better than the CY in terms of comminution of the mill charge. Crystallite sizes for selected $\omega/\Omega + 1$ are reported in Table 2.

4.2. Effect of jar shape on milling time

Experimental data reported in Fig. 7 were produced from samples ground in the jars for 32 h, a milling time that previous studies [18] demonstrated to be optimal to obtain a sufficiently homogeneous end product when using the CY jar. However, this time could be an upper bound for the new design jars, showing higher efficiency in comminution than the CY.

To validate this hypothesis, the CY and the HM jars (the latter chosen as representative of all the new design jars) were exper-

impacts with high normal velocity component, which are the most effective in the comminution of brittle materials.

Validation of these predictions was addressed by WPPM analysis of experimental XRPD patterns collected for fluorite samples ground for 32 h under different velocity ratios, suppling the average crystallite dimensions $\langle D \rangle$ of the end-products. A selection of representative XRPD patterns of fluorite ground with Ω =

Table 2
Average crystallite size $\langle D \rangle$ for the fine and coarse fractions. Selected $\omega/\Omega + 1$ with Ω=200 rpm are reported.

$\omega/\Omega + 1$	$\langle D \rangle$ Fine, nm			$\langle D \rangle$ Coarse, nm		
	−1.0	−1.8	−2.6	−1.0	−1.8	−2.6
Cy	5.0	8.9	10.8	60.7	–	–
Hm	10.5	8.5	3.8	–	–	297.0
1l	12.4	11.7	10.0	20.4	–	28.3
3l	11.1	12.0	9.3	–	–	242.3
t	11.2	11.2	9.6	–	–	216.7
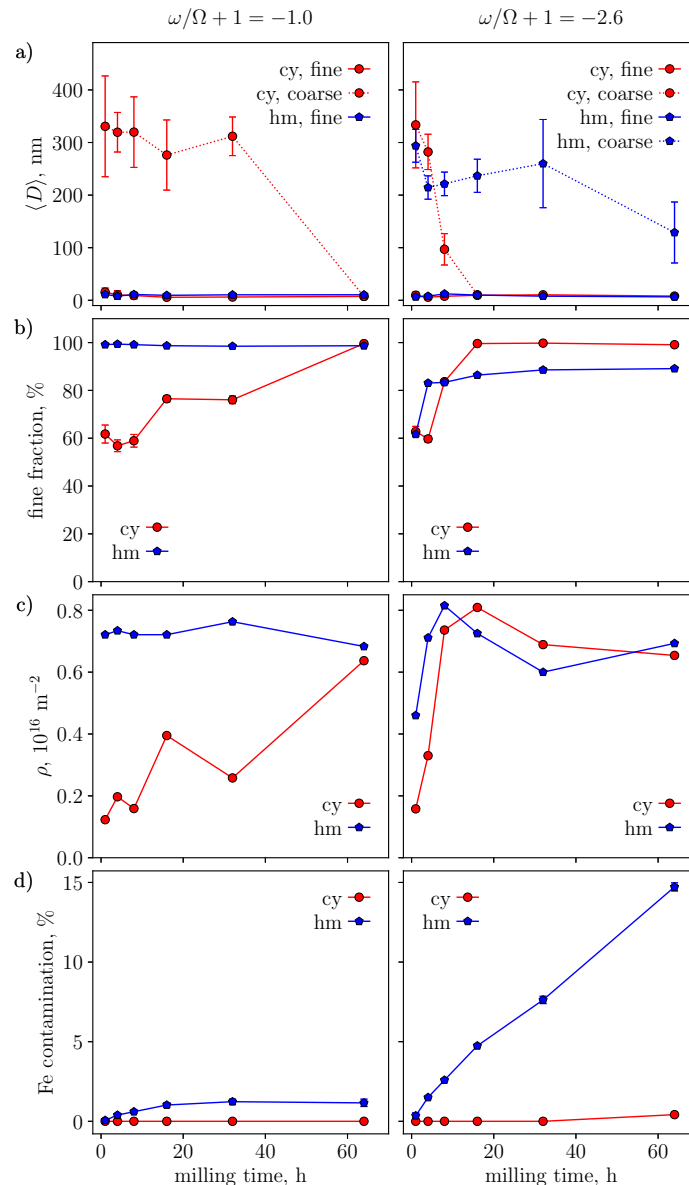
Fig. 8. LPA data for calcium fluoride milled in the CY and the HM jars for different milling times and $\omega/\Omega + 1 = -1.0$ (left), -2.6 (right) velocity ratios. Data reported as a function of milling time are (a) the mean domain size $\langle D \rangle$, (1 or 2 distinct distributions of sizes were necessary to properly model the data depending on the inhomogeneity of the powders; particularly the HM produces a homogeneous fine fraction and therefore only this curve is reported), (b) percentage of fine fraction, (c) average dislocation density ρ and (d) iron contamination percentage.

imentally tested under six different milling times (1 h, 4 h, 8 h, 16 h, 32 h and 64 h). Experiments with fluorite were performed for two velocity ratios, namely $\omega/\Omega + 1 = -1.0$ and $\omega/\Omega + 1 = -2.6$, the former being within the range of ideal milling condi-

tions for the HM and the latter favourable to the CY. XRPD-LPA results are reported in Fig. 8 in terms of (a) mean domain size $\langle D \rangle$ (b) percentage of fine fluorite fraction, (c) average dislocation density ρ and (d) iron contamination percentage.

For the condition $\omega/\Omega + 1 = -1.0$, Fig. 8 (a, b left) demonstrates that for milling time shorter than or equal to 32 h, the CY jar gives a non-homogeneous end product, with a relevant coarse fraction of several hundred nanometres of mean domain size. On the contrary, the HM jar produces a single fluorite phase, uniformly and finely ground, even after short milling time (e.g. 1 h).

At $\omega/\Omega + 1 = -2.6$ (Fig. 8, a, b right) the rolling regime establishes in the HM jar which is reflected in an end product with a fraction of coarse grains persisting also for prolonged milling time (e.g. 64 h). A more uniform fine powder is instead delivered by the CY – operating under best milling conditions – although a grinding time of at least 16 h is required.

Therefore it should be highlighted that, when operating under favourable mill configuration, the HM jar (as well as the other new design jars) needs much shorter milling time than the CY to produce a well-ground end product. Jars with modified shape can therefore shorten the overall duration of the grinding process, saving time and energy.

Besides size reduction, XRPD-LPA provided information on the dislocation density ρ produced by the two jars, reported in Fig. 8c. It can be seen that at $\omega/\Omega + 1 = -1.0$, the HM jar immediately engenders a high dislocation density which is then constant as a function of milling time, whereas for the CY it increases with time. For $\omega/\Omega + 1 = -2.6$ instead, for both jars this quantity steeply grows in the first 8 h.

Fig. 8d also highlights the influence of the milling time on the iron contamination from the grinding media. This phenomenon should be carefully considered since, during the grinding process, wear of the milling media and/or the jar is inevitably engendered by mutual friction and collisions. Debris are mixed with the charge, leading to the contamination of the final product [1,22,46]. While in a few cases wear has been demonstrated to play a positive role by introducing reagents or catalysts [47,46], in general it deteriorates the quality of the end-product, to the point that sometimes it must be removed in a post-process step [48,49]. Several strategies have been proposed in literature to limit or even avoid this side effect, the most immediate being the careful selection of jar and balls materials [1,50] (e.g. using – when possible – the same material for the milling media and the mill feed to eliminate cross-contamination).

Wear is intuitively expected to increase with milling time and Fig. 8c shows that for extended grinding the HM produces a larger fraction of iron than the CY jar, most likely because of the correspondingly larger fraction of normal impacts taking place in the former jar shape. However, results evidence that the milling time required to produce a finely ground powder is quite short when HM operates at optimal velocity ratio (e.g. $\omega/\Omega + 1 = -1.0$), and in this condition contamination is almost absent or comparable with that developed by grinding the same powder in a CY jar for 32 h. It can therefore be concluded that adopting the new design jars is a viable solution to produce finely comminuted and homogeneous powders with limited contamination, with the advantage of a process time much shorter than required by conventional ball milling jars.

5. Conclusions

Four new designs of the internal shape of the planetary ball mill jar were designed to enhance comminution efficiency of the grinding process. This was achieved by introducing different obstacles along the surface of the standard cylindrical vial. The new jars were investigated by multibody dynamics simulations validated by operando video recordings of the milling process for different $\omega/\Omega + 1$ velocity ratios. Simulations and camera movies showed that the new designs promote the detachment of the balls from the jar wall, increasing the disorder of ball motion with respect to the trajectories in the traditional CY jar. This causes an increase (i) of the number of high normal-velocity impacts, especially effective in the comminution of brittle materials, and (ii) of the average normal impact energy available, from $\omega/\Omega + 1 = -0.0$ to -2.6, when balls start to roll along jar wall. XRPD-LPA, providing insights on the average crystallite size of the end product, was performed on ground calcium fluoride and validated simulation predictions. Indeed, starting from low velocity ratios and for a broader range of values than the standard CY, new design jars showed higher efficiency, providing a finer and more homogeneous end product. The analysis shows that jar shape also influences other characteristics of the end product such as defect content and contamination. Therefore the choice of the most suitable jar strictly depends on the specific target of the milling process. For example, for a finely ground and homogeneous end product presenting low contamination and defectivity, the HM jar operating at $\omega/\Omega + 1 = -1.0$ and Ω=200 rpm can be a proper choice.

Finally, the effect of milling time was investigated for the CY and the HM jars, the latter chosen as representative of the new design jars. LPA of calcium fluoride milled for different times pointed out that the HM jar yields a well ground end product in milling time as short as 1 h, whereas the traditional CY requires at least 16 h to give a similar result, even when best operating conditions are used. Jar shape is therefore a crucial variable for the reduction of time and energy required by the milling process.

Acknowledgements

Appendix A. Supplementary material

Supplementary data associated with this article can be found, in the online version, at https://doi.org/10.1016/j.apt.2020.04.027.

References

[1] C.F. Burmeister, A. Kwade, Process engineering with planetary ball mills, Chem. Soc. Rev. 42 (2013) 7660–7667, https://doi.org/10.1039/C3CS35455E.

[2] M. D'Incau, M. Leoni, P. Scardi, High-energy grinding of FeMo powders, J. Mater. Res. 22 (2007) 1744–1753, https://doi.org/10.1557/JMR.2007.0224.

[3] V. Šepelák, S. Bégin-Colin, G. Le Caër, Transformations in oxides induced by high-energy ball-milling, Dalton Trans. 41 (2012) 11927–11948, https://doi.org/10.1039/C2DT30349C.

[4] A. Stolle, T. Szuppa, S.E.S. Leonhardt, B. Ondruschka, Ball milling in organic synthesis: solutions and challenges, Chem. Soc. Rev. 40 (2011) 2317–2329, https://doi.org/10.1039/C0CS00195C.

[5] I. Colombo, G. Grassi, M. Grassi, Drug mechanochemical activation, J. Pharm. Sci. 98 (11) (2009) 3961–3986, https://doi.org/10.1002/jps.21733.

[6] E. Cappelletto, L. Rebuffi, A. Flor, P. Scardi, Microstructural effects of high-energy grinding on poorly soluble drugs: the case study of Efavirenz, Powder Diffr. (2017) 1–6, https://doi.org/10.1017/S0885715617000161.

[7] VV.AA., High-Energy Ball Milling: Mechanochemical Processing of Nanopowders, Woodhead Publishing, 2010.

[8] P.L. Brun, L. Froyen, L. Delaey, The modelling of the mechanical alloying process in a planetary ball mill: comparison between theory and in-situ observations, Mater. Sci. Eng.: A 161 (1) (1993) 75–82, https://doi.org/10.1016/0921-5093(93)90477-V.

[9] S. Rosenkranz, S. Breitung-Faes, A. Kwade, Experimental investigations and modelling of the ball motion in planetary ball mills, Powder Technol. 212 (1) (2011) 224–230, https://doi.org/10.1016/j.powtec.2011.05.021.

[10] A. Rogachev, D. Moskovskikh, A. Nepapushev, T. Sviridova, S. Vadchenko, S. Rogachev, A. Mukasyan, Experimental investigation of milling regimes in planetary ball mill and their influence on structure and reactivity of gasless powder exothermic mixtures, Powder Technol. 274 (2015) 44–52, https://doi.org/10.1016/j.powtec.2015.01.009.

[11] N. Burgio, A. Iasonna, M. Magini, S. Martelli, F. Padella, Mechanical alloying of the Fe–Zr system. correlation between input energy and end products, Il Nuovo Cimento 13 (4) (1991) 459–476, https://doi.org/10.1007/BF02452130.

[12] H. Mio, J. Kano, F. Saito, K. Kaneko, Effects of rotational direction and rotation-to-revolution speed ratio in planetary ball milling, Mater. Sci. Eng.: A 332 (1–2) (2002) 75–80, https://doi.org/10.1016/S0921-5093(01)01718-X.

[13] F. Schneider, A. Stolle, B. Ondruschka, H. Hopf, The suzuki - miyaura reaction under mechanochemical conditions, Organ. Process Res. Develop. 13 (1) (2009) 44–48, https://doi.org/10.1021/op800148y, arXiv:10.1021/op800148y.

[14] T. Szuppa, A. Stolle, B. Ondruschka, W. Hopfe, Solvent-free dehydrogenation of [gamma]-terpinene in a ball mill: investigation of reaction parameters, Green Chem. 12 (2010) 1288–1294, https://doi.org/10.1039/C002819C.

[15] M. Matsuoka, J. Hirata, S. Yoshizawa, Kinetics of solid-state polymorphic transition of glycine in mechano-chemical processing, Chem. Eng. Res. Des. 88 (9) (2010) 1169–1173, https://doi.org/10.1016/j.cherd.2010.01.011.

[16] H. Mio, J. Kano, F. Saito, K. Kaneko, Optimum revolution and rotational directions and their speeds in planetary ball milling, Int. J. Miner. Process. 74 (2004) S85–S92, special Issue Supplement Comminution 2002. doi:10.1016/j.minpro.2004.07.002.

[17] M. Broseghini, M. D'Incau, L. Gelisio, N. Pugno, P. Scardi, Effect of jar shape on high-energy planetary ball milling efficiency: Simulations and experiments, Mater. Des. 110 (2016) 365–374, https://doi.org/10.1016/j.matdes.2016.06.118.

[18] M. D'incau, High energy milling in nanomaterials technologies: process modelling and optimization, Ph.D. thesis, University of Trento, 2008.

[19] P. Baláz, M. Achimovičová, M. Baláz, P. Billik, Z. Cherkezova-Zheleva, J.M. Criado, F. Delogu, E. Dutková, E. Gaffet, F.J. Gotor, R. Kumar, I. Mitov, T. Rojac, M. Senna, A. Streletskii, K. Wieczorek-Ciurowa, Hallmarks of mechanochemistry: from nanoparticles to technology, Chem. Soc. Rev. 42 (2013) 7571–7637, https://doi.org/10.1039/C3CS35468G.

[20] S. Chauruka, A. Hassanpour, R. Brydson, K. Roberts, M. Ghadiri, H. Stitt, Effect of mill type on the size reduction and phase transformation of gamma alumina, Chem. Eng. Sci. 134 (2015) 774–783, https://doi.org/10.1016/j.ces.2015.06.004.

[21] M.V. Antisari, A. Montone, N. Jovic, E. Piscopiello, C. Alvani, L. Pilloni, Low energy pure shear milling: A method for the preparation of graphite nano-sheets, Scripta Mater. 55 (11) (2006) 1047–1050, https://doi.org/10.1016/j.scriptamat.2006.08.002.

[22] C. Suryanarayana, Mechanical alloying and milling, Prog. Mater Sci. 46 (1–2) (2001) 1–184, https://doi.org/10.1016/S0079-6425(99)00010-9.

[23] Fritsch Vario-Planetary Mill PULVERISETTE 4, <http://www.fritsch-milling.com/products/milling/planetary-mills/pulverisette-4-classic-line/description/>.

[24] MSC Adams, <http://www.mscsoftware.com/it/product/adams>.

[25] M. Broseghini, L. Gelisio, M. D'Incau, C.A. Ricardo, N. Pugno, P. Scardi, Modeling of the planetary ball-milling process: The case study of ceramic powders, J. Eur. Ceram. Soc. 36 (9) (2016) 2205–2212, https://doi.org/10.1016/j.jeurceramsoc.2015.09.032.

[26] H.M. Lankarani, P.E. Nikravesh, Continuous contact force models for impact analysis in multibody systems, Nonlinear Dyn. 5 (2) (1994) 193–207, https://doi.org/10.1007/BF00045676.

[27] S. Dubowsky, F. Freudenstein, Dynamic analysis of mechanical systems with clearances – part 1: Formation of dynamic model, J. Eng. Indust. 93 (1) (1971) 305–309, https://doi.org/10.1115/1.3427895.

[28] W. Goldsmith, Impact: the theory and physical behaviour of colliding solids, Dover Publications, 2001.

[29] M. Broseghini, Modelling of high-energy grinding processes, Ph.D. thesis, University of Trento, 2017.

[30] H.M. Hilber, T.J.R. Hughes, R.L. Taylor, Improved numerical dissipation for time integration algorithms in structural dynamics, Earthquake Eng. Struct. Dynam. 5 (3) (1977) 283–292, https://doi.org/10.1002/eqe.4290050306.

[31] D. Negrut, R. Rampalli, G. Ottarsson, A. Sajdak, On an implementation of the Hilber-Hughes-Taylor method in the context of index 3 differential-algebraic equations of multibody dynamics (detc2005-85096), J. Comput. Nonlinear Dyn. 2 (1) (2006) 73–85, https://doi.org/10.1115/1.2389231.

[32] VV.AA., Defect and Microstructure Analysis by Diffraction, Oxford University Press, 1999.

[33] VV. AA., Diffraction Analysis of the Microstructure of Materials, Springer, 2004.

[34] M. Broseghini, M. D'Incau, L. Gelisio, N. Pugno, P. Scardi, Homogeneity of ball milled ceramic powders: effect of jar shape and milling conditions, Data in Brief 10 (2017) 186–191, https://doi.org/10.1016/j.dib.2016.11.070.

[35] P. Scardi, Microstructural properties: Lattice defects and domain size effects, in: R. Dinnebier, S. Billinge (Eds.), Powder Diffraction. Theory and practice, RSC Publishing, Cambridge, 2008, pp. 378–416, Ch. 13.

[36] P. Scardi, M. Leoni, Diffraction line profiles from polydisperse crystalline systems, Acta Crystallogr. Sect. A 57 (5) (2001) 604–613, https://doi.org/10.1107/S0108767301008881.

[37] P. Scardi, M. Leoni, Whole powder pattern modelling, Acta Crystallogr. Sect. A 58 (2) (2002) 190–200, https://doi.org/10.1107/S0108767301021298.

[38] E. Hellstern, H.J. Fecht, Z. Fu, W.L. Johnson, Structural and thermodynamic properties of heavily mechanically deformed ru and alru, J. Appl. Phys. 65 (1) (1989) 305–310, https://doi.org/10.1063/1.342541.

[39] J. Huang, Y. Wu, H. Ye, Ball milling of ductile metals, Mater. Sci. Eng.: A 199 (2) (1995) 165–172, https://doi.org/10.1016/0921-5093(94)09715-1.

[40] Á. Révész, T. Ungár, A. Borbély, J. Lendvai, Dislocations and grain size in ball-milled iron powder, Nanostruct. Mater. 7 (7) (1996) 779–788, https://doi.org/10.1016/S0965-9773(96)00048-7.

[41] L. Börner, J. Eckert, Nanostructure formation and steady-state grain size of ball-milled iron powders, Materials Science and Engineering: A 226 (1997) 541 – 545, ninth International Conference on Rapidly Quenched and Metastable Materials. doi:10.1016/S0921-5093(97)80063-9.

[42] S. Vives, E. Gaffet, C. Meunier, X-ray diffraction line profile analysis of iron ball milled powders, Mater. Sci. Eng.: A 366 (2) (2004) 229–238, https://doi.org/10.1016/S0921-5093(03)00572-0.

[43] O. Boytsov, A. Ustinov, E. Gaffet, F. Bernard, Correlation between milling parameters and microstructure characteristics of nanocrystalline copper powder prepared via a high energy planetary ball mill, J. Alloy. Compd. 432 (2007) 103–110, https://doi.org/10.1016/j.jallcom.2006.05.101.

[44] Topas-Academic, <http://www.topas-academic.net>.

[45] A. Kwade, Mill selection and process optimization using a physical grinding model, International Journal of Mineral Processing 74 (2004) S93–S101, special Issue Supplement Comminution 2002. doi:10.1016/j.minpro.2004.07.027.

[46] F.K. Urakaev, Mineral processing by the abrasive-reactive wear, Int. J. Miner. Process. 92 (1) (2009) 58–66, https://doi.org/10.1016/j.minpro.2009.02.010.

[47] D.A. Fulmer, W.C. Shearouse, S.T. Medonza, J. Mack, Solvent-free sonogashira coupling reaction viahigh speed ball milling, Green Chem. 11 (2009) 1821–1825, https://doi.org/10.1039/B915669K.

[48] V.P. Balema, J.W. Wiench, M. Pruski, V.K. Pecharsky, Solvent-free mechanochemical synthesis of phosphonium salts, Chem. Commun. (2002) 724–725, https://doi.org/10.1039/B111515D.

[49] A. Sato, J. Kano, F. Saito, Analysis of abrasion mechanism of grinding media in a planetary mill with dem simulation, Adv. Powder Technol. 21 (2) (2010) 212–216, https://doi.org/10.1016/j.apt.2010.01.005.

[50] E. Ivanov, C. Suryanarayana, Materials and process design through mechanochemical routes, J. Mater. Synth. Process. 8 (3) (2000) 235–244, https://doi.org/10.1023/A:1011372312172.